Journal of
Applied Remote Sensing

RemoteSensing.SPIEDigitalLibrary.org

Electromagnetic scattering and Doppler spectrum simulation of time-varying oil-covered nonlinear sea surface

Pengju Yang
Lixin Guo
Chungang Jia

SPIE.

Electromagnetic scattering and Doppler spectrum simulation of time-varying oil-covered nonlinear sea surface

Pengju Yang,* Lixin Guo, and Chungang Jia
Xidian University, School of Physics and Optoelectronic Engineering, No. 2 South Taibai Road, Xi'an, Shaanxi 710071, China

Abstract. Based on the model of Lombardini et al. [*J. Atmos. Ocean. Technol.* **6**(6), 882–890 (1989)], which can predict the hydrodynamic damping of rough sea surfaces in the presence of oil films, the influence of sea slicks on the sea surface roughness spectrum and sea surface geometrical structure is examined briefly in the present study. On this basis, the influence of sea slicks on the angular distribution of the bistatic scattering coefficient of sea surfaces and the Doppler spectrum signature of backscattered radar sea-echo is investigated in detail based on a frequency-domain numerical method of the parallel fast multiple method. Simulation results show that Doppler spectrum signatures including Doppler shift and spectral bandwidth of radar sea-echo are significantly affected by sea slicks, which are qualitatively consistent with wave-tank or open sea measurements. Moreover, simulation results indicate that the Doppler spectrum signature is a promising technique for remote sensing of oil films floating on sea surfaces. [DOI: 10.1117/1.JRS.10.016015]

Keywords: electromagnetic scattering; Doppler spectrum; oil-covered sea surface; time-varying sea surface.

Paper 15337 received May 18, 2015; accepted for publication Jan. 27, 2016; published online Feb. 19, 2016.

1 Introduction

In the past decades, the problem of remote sensing of oil spills floating on rough sea surfaces was investigated experimentally and theoretically, and most of the research effort on this topic was devoted to analyzing and processing remote sensing data, particularly by synthetic aperture radar.[1–5] Electromagnetic (EM) scattering modeling of oil spills floating on rough sea surfaces was also presented in Refs. 6–9, which serves as a basis for remote sensing of oil spills floating on a rough ocean surface and actually involves the investigation of EM scattering from stratified rough surfaces.[10–13] As a promising technique in many areas such as ocean wave spectra estimation, sea surface wind speed retrieval, ocean wave parameters extraction, and sea surface current measurement, the Doppler spectrum of backscattered echoes from a time-evolving sea surface carries much more information than the normalized radar cross-section of the sea surface[14–17] and proves to be a much more precise and sensitive tool for monitoring fluid motion. Most of the existing literature on this topic concentrated primarily on the hydrodynamic nonlinear interactions between ocean waves on the Doppler spectrum of time-varying clean ocean surfaces,[18–21] in which a broadening of Doppler spectra of the nonlinear sea surface and a separation of Doppler spectra between vertical and horizontal polarizations for nonlinear sea surfaces are observed, especially at low grazing angles.

Motivated by the fact that oil slicks strongly damp the capillary waves of sea surfaces and inherently change the sea surface geometrical structure, this paper is devoted mainly to an investigation of EM scattering features and Doppler spectrum signatures of oil films floating on time-varying one-dimensional (1-D) dielectric sea surfaces, which is potentially valuable for remote sensing of sea slicks floating on ocean surfaces. In the present study, the nonlinear model termed as the choppy wave model (CWM) is utilized for describing nonlinear interactions between

*Address all correspondence to: Pengju Yang, E-mail: pjyang@yeah.net

1931-3195/2016/$25.00

ocean waves,[22] which are extremely important for the Doppler spectrum of radar sea-echo, especially at low grazing angles. The simulation results in the present study indicate that the scattering intensity in the vicinity of the specular direction is increased, whereas the scattering intensity away from the specular direction is decreased due to the presence of sea slicks, which are qualitatively consistent with measurements.[23–26] The simulation results also show that the Doppler shift in the presence of sea slicks can decrease or increase, dependent on incidence angles and oil characteristics, which is qualitatively consistent with open sea measurements performed at a fixed incidence angle.[27,28] In addition, a narrowing of the Doppler spectrum in the presence of oil slicks is observed, which is qualitatively consistent with wave-tank measurements.[29]

The remainder of this paper is organized as follows. In Sec. 2, the influence of oil films' damping on the sea surface roughness spectrum and sea surface geometrical structure is examined based on the model of Lombardini et al., and the formulation of EM scattering from two-layered rough surfaces and the simulation procedures of the Doppler spectrum are presented. The numerical results of the bistatic scattering coefficient and the Doppler spectra of backscattered echoes from oil-free and oil-covered sea surfaces are discussed in Sec. 3. Section 4 concludes this paper.

2 Theoretical Model

2.1 *Modeling of Contaminated Sea Surface*

In the existing literature, there are only a few models that can take into account oil films and predict the hydrodynamic damping of rough sea surfaces in the presence of surface oil films.[30–32] Since the emphasis of the present study is on the influence of natural or organic sea slicks on the Doppler spectrum of backscattered echoes from sea surfaces, the model of Lombardini et al.[32] is considered in this paper. Actually, the model of Lombardini et al. is independent of oil films' thickness and is only valid for thin oil films. According to the model proposed by Lombardini et al., the roughness spectrum of an oil-covered sea surface S_{cont} is related to the clean sea surface roughness spectrum S_{clean} by the following ratio:[9,32]

$$S_{\text{cont}}(k;u,E_0,\omega_D)=\frac{S_{\text{clean}}(k,u)}{y_s(k;E_0,\omega_D)}, \tag{1}$$

where y_s is the damping ratio.

This paper considers only the insoluble films and a fully covered sea, and thus, the damping ratio y_s is expressed by

$$y_s(f,E_0,\omega_D)=\frac{1-2\tau+2\tau^2-X+Y(X+\tau)}{1-2\tau+2\tau^2-2X+2X^2}, \tag{2}$$

where

$$\tau=\left(\frac{\omega_D}{2\omega}\right)^{\frac{1}{2}} \quad X=\frac{E_0k^2}{\rho(2\nu\omega^3)^{0.5}} \quad Y=\frac{E_0k}{4\rho\nu\omega} \tag{3}$$

are dimensionless quantities and

$$f=\frac{\omega}{2\pi}=\frac{(\varsigma k^3/\rho+gk)^{1/2}}{2\pi} \tag{4}$$

is the dispersion law. In Eqs. (2)–(4), ρ is the water density, g is the acceleration of gravity, $\nu=10^{-6}$ m/s is the kinematic viscosity, and $\varsigma=74\times10^{-3}$ N/m is the surface tension. E_0 denotes the elasticity modulus, and ω_D represents a characteristic frequency. This paper considers three types of oil films with parameters $\{\omega_{\text{D}}=6\text{ rad/s}, E_0=9\text{ mN/m}\}$, $\{\omega_{\text{D}}=13\text{ rad/s}, E_0=18\text{ mN/m}\}$, and $\{\omega_{\text{D}}=11\text{ rad/s}, E_0=25\text{ mN/m}\}$, respectively. It needs to be noted that these values were retrieved from experiments conducted in the Sicilian Channel and the Gulf of Maine.[32]

To take into account the small-scale waves of the sea surface, the sea surface roughness spectrum proposed by Elfouhaily et al. is used in the present study for describing the clean sea surface, which consists of the gravity waves spectrum and capillary waves spectrum and can be expressed as[33]

$$S_{\text{clean}}(k) = k^{-3}[B_L(k) + B_H(k)], \tag{5}$$

where B_L denotes the long-wave curvature spectrum and B_H represents the short-wave curvature spectrum. The detailed expressions of B_L and B_H can be found in Ref. 33, which is not presented here due to space limitations.

With the knowledge of the sea surface roughness spectrum, the RMS slope and the RMS height can be derived as

$$\sigma_s = \sqrt{\int_0^{+\infty} \mathrm{d}k k^2 S(k)}, \qquad h = \sqrt{\int_{-\infty}^{\infty} \mathrm{d}k S(k)}, \tag{6}$$

where $S(k)$ can be either $S_{\text{clean}}(k)$ or $S_{\text{cont}}(k)$. The RMS height and RMS slope of a clean and a contaminated sea with Elfouhaily spectrum can be calculated numerically with the Elfouhaily spectrum being truncated. In the following EM simulations, we fixed the cutoff to be five times the electromagnetic wavenumber, that is, $K_c = 5k_0$, with k_0 being the wavenumber of the incident electromagnetic wave in free space, which definitely includes all potential Bragg scatterers.

The two air/oil and oil/sea interfaces are strongly correlated and can be regarded as fully correlated (i.e., identical) for thin oil films up to a few millimeters; hence, the two interfaces of oil films can be considered as locally plane parallel interfaces as in Ref. 9. Therefore, in the present study, the contaminated and clean sea surfaces are generated as realizations of a Gaussian random process with the contaminated sea surface roughness spectrum S_{cont} and the clean sea surface roughness spectrum S_{clean}, respectively. The CWM surface model describing nonlinear interactions between ocean waves is utilized in this paper to investigate the influence of sea surface nonlinearities on the Doppler spectrum, which is based on a Lagrangian description of ocean waves and can be constituted by horizontal displacement of the Hilbert transform of a reference linear surface.[22]

Figures 1(a) and 1(b) present the roughness spectra of oil-free and oil-covered sea surfaces with wind speeds of $U_{10} = 3$ m/s and $U_{10} = 5$ m/s, respectively. The wind fetch is set to 30 km. It should be noted that for ocean waves whose frequency is smaller than 1 Hz, the influence of oil films on the sea surface roughness spectrum is not taken into account as illustrated in Ref. 32. From Fig. 1, we can observe that the higher-frequency components corresponding to capillary waves of sea surfaces are significantly affected by oil films' damping effect. Moreover, the oil film with parameter $\{\omega_{\text{D}} = 11 \text{ rad/s}, E_0 = 25 \text{ mN/m}\}$ has a stronger damping effect on the sea surface roughness spectrum compared with the oil films with parameters $\{\omega_{\text{D}} = 13 \text{ rad/s}, E_0 = 18 \text{ mN/m}\}$ and $\{\omega_{\text{D}} = 6 \text{ rad/s}, E_0 = 9 \text{ mN/m}\}$.

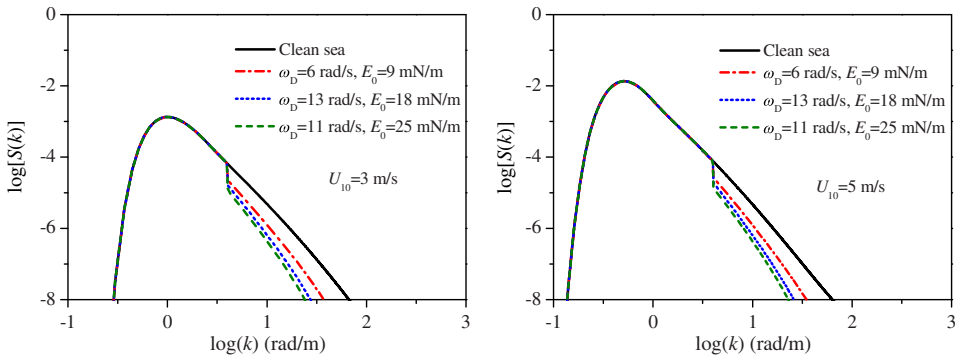

Fig. 1 Roughness spectra of oil-free and oil-covered sea surface versus the wavenumber: (a) $U_{10} = 3$ m/s and (b) $U_{10} = 5$ m/s.

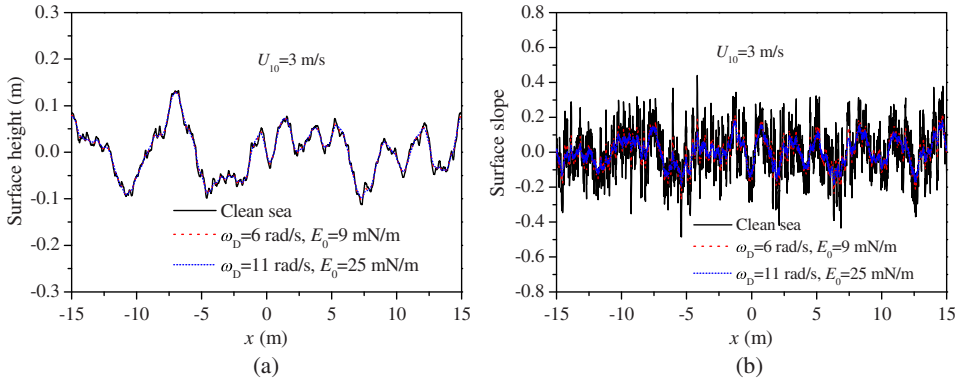

Fig. 2 Geometrical structure comparison between a clean and an oil-covered linear sea surface: (a) sea surface height profile comparison and (b) sea surface slope comparison.

The damping effect of oil films inherently has an influence on the sea surface geometrical structure as well as sea surface statistical characteristics, as illustrated in Figs. 2 and 3. The surface height and slope of a realization of clean and contaminated sea surfaces are presented in Figs. 2(a) and 2(b), respectively. Comparing Figs. 2(a) and 2(b), we can observe that sea surface heights are slightly affected by oil films, whereas sea surface slopes are significantly reduced due to the presence of sea slicks. Moreover, sea surface slopes of the oil-covered sea with oil parameter $\{\omega_D = 11$ rad/s, $E_0 =$ mN/m$\}$ are smaller than those with oil films with parameters $\{\omega_D = 6$ rad/s, $E_0 = 9$ mN/m$\}$ and $\{\omega_D = 13$ rad/s, $E_0 = 18$ mN/m$\}$. The comparisons of surface RMS height and RMS slope between clean and contaminated sea surfaces are exhibited in Figs. 3(a) and 3(b), respectively. As expected, surface RMS height is almost not affected by oil films' damping as illustrated in Fig. 3(a), whereas surface RMS height is significantly reduced by oil films' damping as depicted in Fig. 3(b).

2.2 *Scattering and Doppler Spectrum Calculation*

The investigation on the Doppler spectra of backscattered echoes from oil-covered sea surfaces involves the calculation of EM scattering from 1-D two-layered rough surfaces as illustrated in Fig. 4. Applying Green's theorem to the three media regions divided by the two rough interfaces Ω_0, Ω_1, and Ω_2, respectively, the coupling integral equations for calculating EM scattering from the 1-D two-layered dielectric rough surface in the three media can be written as[34]

$$\psi_{\text{inc}}(\bar{r}) = \frac{1}{2}\psi_0(\bar{r}) - \int_{S_1} \mathrm{d}S'[\psi_0(\bar{r}')\hat{n}_1' \cdot \nabla' G_0(\bar{r}, \bar{r}') - G_0(\bar{r}, \bar{r}')\hat{n}_1' \cdot \nabla' \psi_0(\bar{r}')] \qquad \bar{r} \in \Omega_0, \tag{7}$$

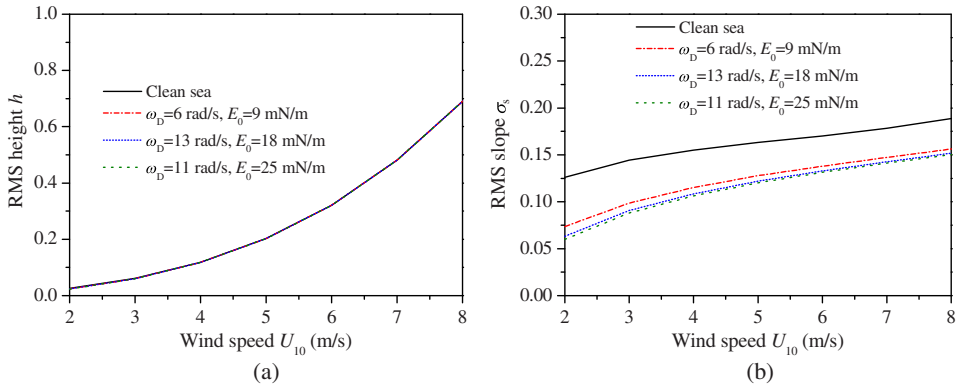

Fig. 3 Statistics comparison between a clean and an oil-covered linear sea surface: (a) RMS height versus the wind speed U_{10} and (b) RMS slope versus the wind speed U_{10}.

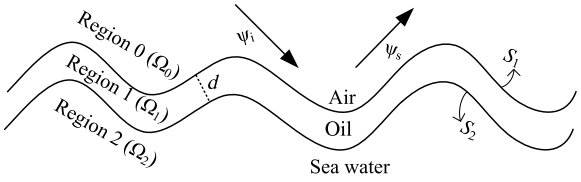

Fig. 4 Geometry of the wave scattering from 1-D rough sea surface covered by oil film.

$$0=\frac{1}{2}\psi_1(\bar{r})+\int_{S_1}\mathrm{d}S'[\psi_1(\bar{r}')\hat{n}_1'\cdot G_1(\bar{r},\bar{r}')-G_1(\bar{r},\bar{r}')\hat{n}_1'\cdot\nabla'\psi_1(\bar{r}')]$$
$$-\int_{S_2}\mathrm{d}S'[\psi_1(\bar{r}')\hat{n}_2'\cdot\nabla' G_1(\bar{r},\bar{r}')-G_1(\bar{r},\bar{r}')\hat{n}_2'\nabla'\psi_1(\bar{r}')] \qquad \bar{r}\in\Omega_1, \tag{8}$$

$$0=\frac{1}{2}\psi_2(\bar{r})+\int_{S_2}\mathrm{d}S'[\psi_2(\bar{r}')\hat{n}_2'\cdot\nabla' G_2(\bar{r},\bar{r}')-G_2(\bar{r},\bar{r}')\hat{n}_2'\cdot\nabla'\psi_2(\bar{r}')] \qquad \bar{r}\in\Omega_2, \tag{9}$$

where $\{G_P(\bar{r},\bar{r}')=(i/4)H_0^{(1)}(k_p|\bar{r}-\bar{r}'|)\}_{p=0,1,2}$ is the Green's function with $H_0^{(1)}(\cdot)$ being the zeroth-order Hankel function of the first kind.

Applying pulse basis functions and points matching procedure to the integral Eqs. (7)–(9) with boundary conditions being used, one can obtain a matrix equation that can be solved by a parallel fast multiple method based on a message passing interface to accelerate calculations of the scattering problem.[34] Upon solving the matrix equation, the surface electric current and surface magnetic current can be obtained. Then the far field can be calculated by utilizing Huygens' principle in terms of the surface currents. The normalized far-field bistatic scattering coefficient (BSC)[35] with the Thorsos tapered plane wave incidence can thus be calculated in terms of the scattered fields.

Frequency-domain methods can be applied to evaluate the EM scattering from a time-evolving sea surface on the basis of a quasi-stationary algorithm,[21,36] which approximately simulates the time-domain problem by repeatedly employing the frequency-domain approach. More precisely, the time-evolving sea can be regarded as time-frozen for a time interval τ if the pulse duration τ is small enough. On the other hand, if the duration τ of such a pulse is large enough and the time-evolving sea still remains time-frozen, the surface illumination can be regarded as a time-harmonic signal, so that we can employ our frequency-domain method to calculate the scattered fields from such a time-frozen sea surface. Then, the scattered signal may be considered as composed of the same pulses of duration τ, whose amplitudes $\psi_s(n\tau,\theta_s;\theta_i)$, $n=0,1,2\ldots$ are determined by solving the frequency-domain integral for each time interval. Apparently, it is crucial to choose an appropriate time duration τ, which has been discussed in detail in Ref. 21.

Based on the simulated time series of backscattered echoes from a time-evolving sea surface, the Doppler spectrum, which is defined as the power spectral density of the random time-varying scattering amplitude, can be evaluated by utilizing a standard spectral estimation technique in terms of the following expression:[21]

$$S(f)=\left\langle\frac{1}{T}\left|\int_0^T\psi(t,\theta_s,\theta_i)e^{-i2\pi ft}\right|^2\right\rangle, \tag{10}$$

where the angular bracket represents the ensemble average over random surface realizations and T denotes the sea surface evolution time. In what follows, we consider only the backscattering case, that is, $\theta_s=-\theta_i$. The procedure of Doppler spectrum simulation can be summarized as follows:

Step 1: Simulate a sequence of time-evolving sea surfaces with time duration τ. If this duration is small enough, the sea surface can be regarded as time-frozen during the time interval τ.

Step 2: Calculate the backscattered field from time-frozen sea surfaces by solving the coupling integral equations to obtain a time series of backscattered echoes from one sea surface realization.

Step 3: Evaluate one realization of the Doppler spectrum by performing a standard spectral estimation technique.
Step 4: Repeat steps 1 through 3 to obtain a number of realizations for the Doppler spectrum, and then take the ensemble average to get an average Doppler spectrum.

In order to quantitatively measure the Doppler spectrum, the Doppler shift f_c, that is, the spectral centroid, and the bandwidth of the Doppler spectrum f_w can be defined by the following expressions, respectively:

$$f_c = \frac{\int f S(f)\mathrm{d}f}{\int S(f)\mathrm{d}f}, \qquad f_w = \sqrt{\frac{\int (f - f_c)^2 S(f)\mathrm{d}f}{\int S(f)\mathrm{d}f}}. \tag{11}$$

3 Numerical Results and Discussion

In the following, numerical simulations are performed at a frequency of $f = 3.0$ GHz. The relative permittivity of sea surface is $\varepsilon_r = 70.4 + i37.6$[37] at a sea water temperature of 25°C and salinity of 30 parts per thousand in terms of the Debye expression, and the relative permittivity of the oil film is taken as $\varepsilon_r^{\mathrm{oil}} = 2.25 + i0.01$.[38] Three types of insoluble homogeneous oil films are considered in this paper, and the mean thickness of oil film d is assumed to be 0.1λ, with λ being the electromagnetic wavelength. In what follows, oil films with parameters $\{\omega_{\mathrm{D}} = 6\ \mathrm{rad/s}, E_0 = 9\ \mathrm{mN/m}\}$, $\{\omega_{\mathrm{D}} = 13\ \mathrm{rad/s}, E_0 = 18\ \mathrm{mN/m}\}$, and $\{\omega_{\mathrm{D}} = 11\ \mathrm{rad/s}, E_0 = 25\ \mathrm{mN/m}\}$ are represented by oil of types A, B, and C, respectively. The Elfouhaily spectrum is utilized for describing the clean sea surfaces, and the Elfouhaily spectrum in conjunction with the model of Lombardini et al. is employed for modeling contaminated sea surfaces. The wind fetch involved in the Elfouhaily spectrum is set to 30 km. The length of sea surface is $L = 204.8\lambda$, and the Thorsos tapered wave with tapering parameter $g = L/6$ is chosen as the incident field to reduce the edge diffraction effect due to the truncation of the rough surface. For Doppler spectra simulation, the criterion for choosing the time interval is discussed in detail in Ref. 21. In the present study, the time step is set to 0.02 and 0.01 s for wind speeds of $U_{10} = 3$ m/s and $U_{10} = 5$ m/s, respectively, to obtain sufficient unambiguous Doppler bandwidth, and each realization of the Doppler spectrum is performed on 256 and 512 time samples for wind speeds of $U_{10} = 3$ m/s and $U_{10} = 5$ m/s, respectively, to obtain sufficient Doppler spectral resolution. The final average Doppler spectra are obtained over 100 ensemble realizations.

Figures 5(a) and 5(b) exhibit the BSC versus scattering angle under incidence angles of $\theta_i = 0$ deg and $\theta_i = 30$ deg for horizontal–horizontal and vertical–vertical (VV) polarizations, respectively. The wind speed at a height of 10 m is $U_{10} = 5$ m/s, and the final BSC is averaged over 100 Monte Carlo realizations. It is readily observed that the angular distribution of the BSC is more concentrated in the vicinity of the specular direction for the oil-covered sea surface than for the oil-free sea surface. This means that BSC decreases more rapidly away from the specular direction for the oil-covered sea than for the oil-free sea surface. One attributes this phenomenon to the fact that an oil-covered sea surface has a lower slope compared with those of an oil-free sea surface, which is due to the difference in the roughness spectrum of the sea surface arising from the damping effect of the oil film. It is also found that the angular distribution of BSC is more concentrated near the specular direction for the oil of type C than for the oil of type A. This can be attributed to the fact that the surface slope of an oil-covered sea with oil film of type C is smaller than those with oil film of type A, which is due to the fact that the damping effect is stronger for oil film of type C than for oil film of type A. For sea surface in the presence of oil films, experimental measurements show that near-nadir backscattering intensity is increased[23,26] and that, at moderate angles of incidence, backscattering power is decreased.[24,25] In Figs. 5(a) and 5(b), we can observe that in the vicinity of the specular direction, BSC in slicks is higher than that of clean sea, and that for the scattering angles away from the specular direction, BSC is much lower than that of clean sea. Hence, our simulation results are qualitatively consistent with measurements.[23–26]

Figure 6 exhibits Doppler spectra of VV-polarized backscattered echoes from clean linear sea, clean nonlinear sea, and contaminated nonlinear sea with wind speed $U_{10} = 3$ m/s at various incidence angles. Oil of type A with parameter $\{\omega_{\mathrm{D}} = 6\ \mathrm{rad/s}, E_0 = 9\ \mathrm{mN/m}\}$ is

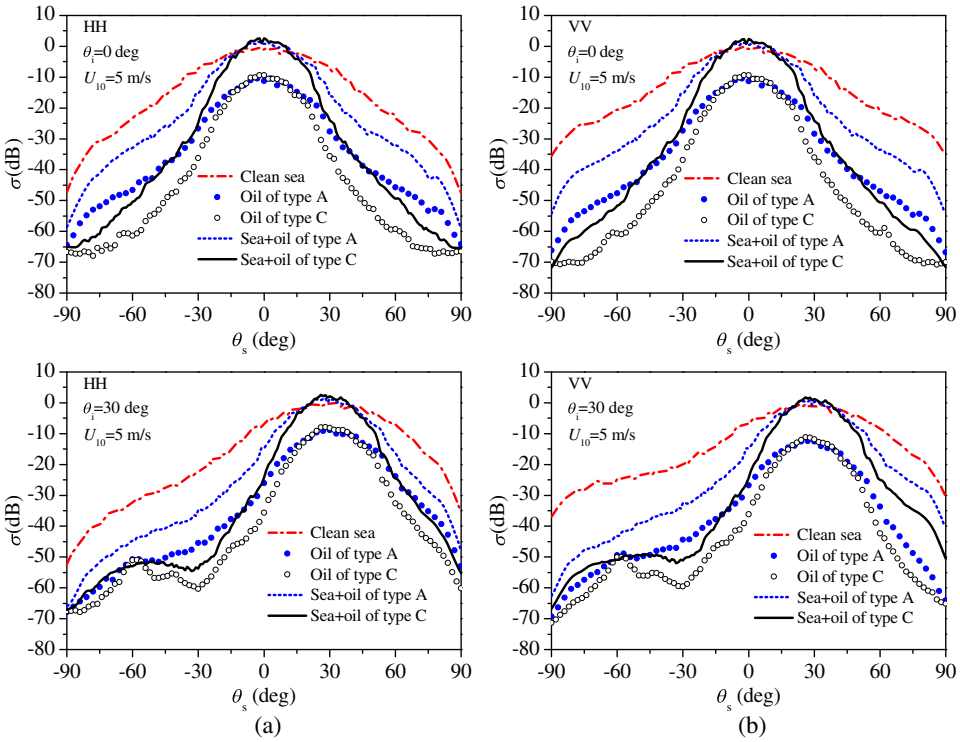

Fig. 5 Bistatic scattering coefficients of clean and contaminated sea for $\theta_i = 0$ deg and $\theta_i = 30$ deg with wind speed $U_{10} = 5$ m/s: (a) horizontal polarization and (b) vertical polarization.

considered in Fig. 6. For reference, the Bragg lines are also plotted with vertical dotted lines, which are predicted by the small perturbation method at first order and are expressed by $f_B = \pm\sqrt{g_0 K_B}/2\pi$, with $K_B(\theta_i) = 2k_0 \sin(\theta_i)$ being the Bragg wavenumber. For linear sea surfaces, it is indicated in Fig. 6 that the Doppler spectrum first becomes broader and then shrinks until it becomes quite narrow when approaching low grazing incidence. In addition, the Doppler spectral peaks of linear sea surfaces locate at higher frequencies compared with the corresponding Bragg shift for small and moderate incidence. As incident angle increases, the Doppler spectral peaks of linear sea surfaces move closer to and eventually coincide with the Bragg shift. This is attributed to the fact that the scattering mechanism is dominated by specular reflection at small incident angles, whereas the Bragg scattering becomes dominant as the incident angle increases.

Comparing the Doppler spectra of clean linear and nonlinear sea surfaces, we can readily observe that at small incidence angles, the difference of Doppler spectrum between clean linear and nonlinear sea surfaces is almost indistinguishable. As incidence angle increases, the difference of Doppler spectrum between clean linear and nonlinear sea surfaces becomes increasingly pronounced, especially at low grazing angles. As illustrated in Fig. 6, the Doppler spectra of nonlinear sea surfaces for low grazing angles are much broader than those of linear sea surfaces. The reason for this difference is that linear sea surface is just a collection of harmonics, each propagating according to a dispersion relation independent of others. It captures the vertical component of orbital motions that shorter waves experience due to long waves by local height changes, but the horizontal component of the orbital velocities of long waves is completely missed due to the neglect of nonlinear interactions between ocean waves. For small incident angles, the line-of-sight projections of sea surface motions are almost entirely due to the vertical components, which are correctly captured by the linear sea surface model. However, the horizontal component of orbital motion starts playing increasingly and then takes a dominant role in the line-of-sight projection as the incidence angle moves toward grazing angles. These back-and-forth motions (nonlinear interactions between ocean waves) are completely missing in the linear sea surface model. The CWM nonlinear sea surface model used in the present study, however, does capture these orbital motions correctly by adding horizontal displacements of the Hilbert transform of a reference linear surface. Obviously, the Doppler spectra of nonlinear sea surfaces

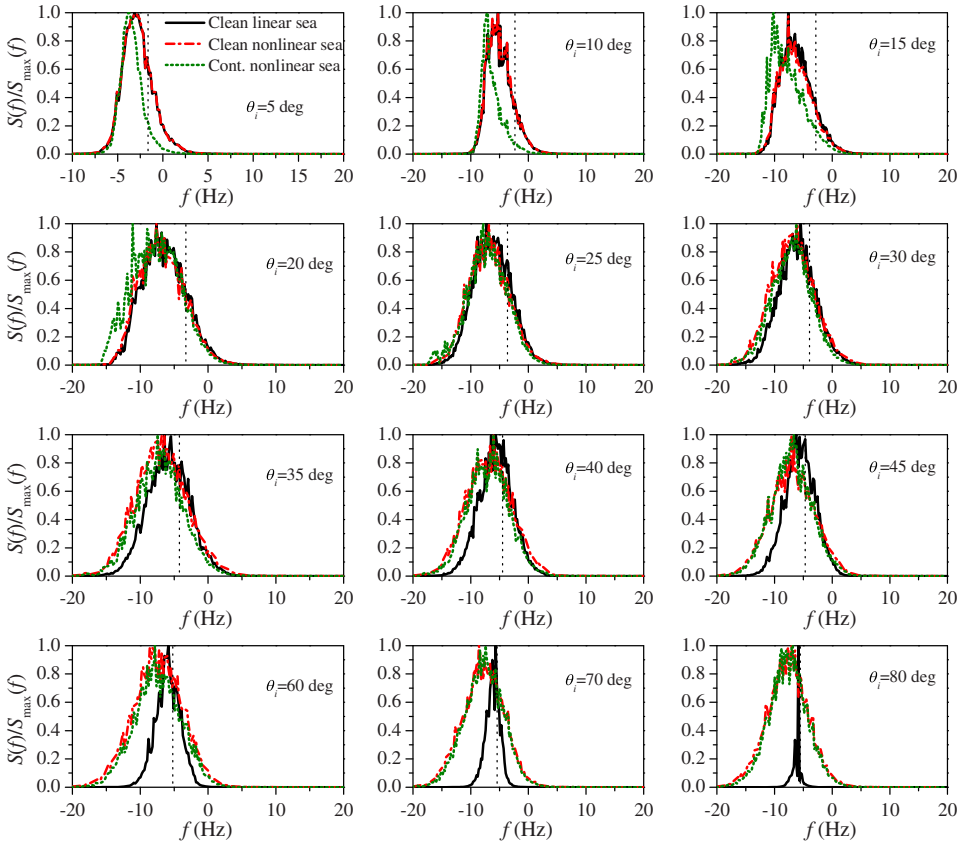

Fig. 6 Average normalized Doppler spectra of backscattered echoes from clean linear sea, clean nonlinear sea, and contaminated nonlinear sea with wind speed $U_{10} = 3$ m/s at various incidence angles. The vertical dotted lines represent Bragg lines.

are more consistent with measurements[39,40] compared with linear sea surfaces. Without considering the nonlinear hydrodynamic interactions between ocean waves, the Doppler spectrum exhibits exceedingly unrealistic behavior toward low grazing angles, degenerating essentially in a narrow Bragg line. Therefore, the CWM nonlinear sea surface model instead of the linear sea surface model is utilized in the present study for modeling realistic sea surfaces. On the basis of the CWM nonlinear sea surfaces, we will investigate the influence of sea slicks on the Doppler spectrum of backscattered radar echoes of sea surfaces.

In Fig. 6, it is indicated that for small incidence angles, the Doppler spectra of contaminated sea surfaces are significantly narrower than those of clean nonlinear sea surfaces. In addition, the Doppler spectral peaks of contaminated sea surfaces are shifted to higher frequencies relative to the corresponding ones of clean sea surfaces. However, as the incidence angle increases, the Doppler spectra of contaminated sea surfaces gradually approach those of clean nonlinear sea surfaces. It should be noted that oil of type A with parameters $\{\omega_D = 6 \text{ rad/s}, E_0 = 9 \text{ mN/m}\}$ is considered in Fig. 6. In comparison with oil of type A, oils of types B and C with parameters $\{\omega_D = 13 \text{ rad/s}, E_0 = 18 \text{ mN/m}\}$ and $\{\omega_D = 11 \text{ rad/s}, E_0 = 25 \text{ mN/m}\}$, respectively, show a stronger damping effect, as illustrated in Sec. 2.1. In what follows, we will discuss the influence of oils of types B and C on the Doppler spectrum of radar echoes from sea surfaces.

Figures 7 and 8 present a comparison of the normalized Doppler spectra of clean and contaminated nonlinear sea surfaces for VV-polarization at various incidence angles with wind speeds $U_{10} = 3$ m/s and $U_{10} = 5$ m/s, respectively. Two types of insoluble homogeneous oils with parameters $\{\omega_D = 13 \text{ rad/s}, E_0 = 18 \text{ mN/m}\}$, denoted as oil B, and $\{\omega_D = 11 \text{ rad/s}, E_0 = 25 \text{ mN/m}\}$, represented by oil C are considered in Figs. 7 and 8, respectively. The Bragg lines are also plotted with vertical dotted lines for reference. Comparing the Doppler

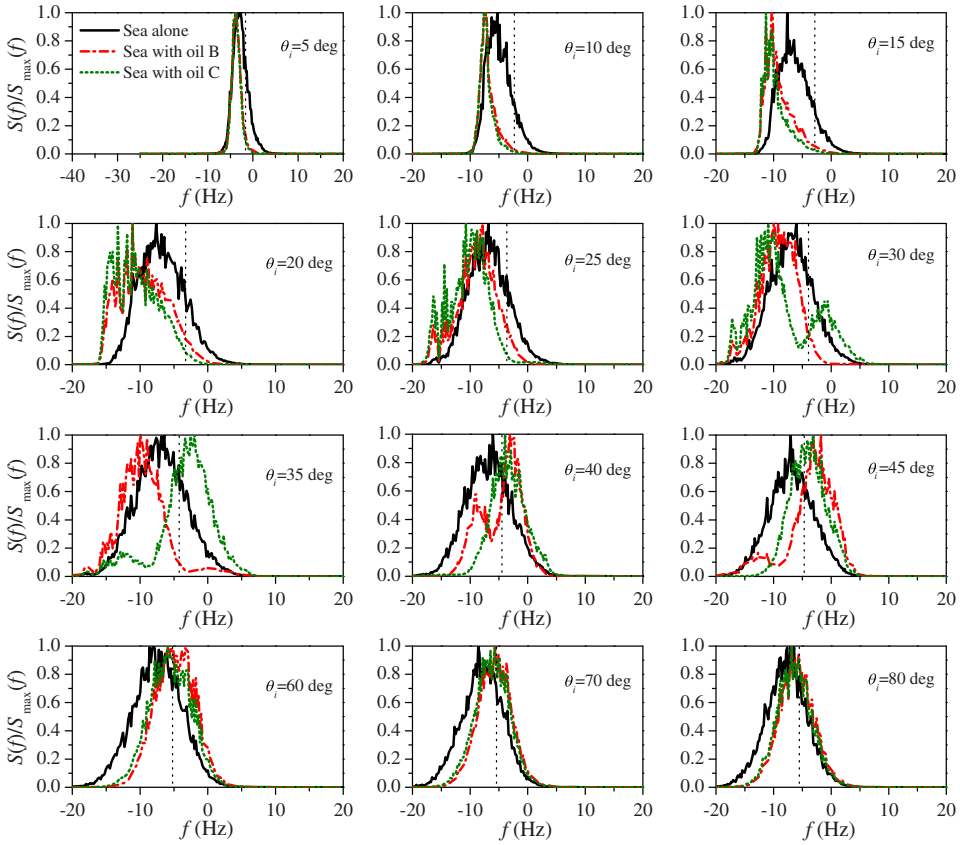

Fig. 7 Comparison of normalized Doppler spectra of backscattered echoes from clean and two types of contaminated nonlinear sea surface with wind speed $U_{10} = 3$ m/s at various incidence angles. The vertical dotted lines represent Bragg lines.

spectra of clean and contaminated sea surfaces, we can observe that the influence of sea slicks on the Doppler spectrum of radar sea-echo is noticeable. More specifically, a narrowing of Doppler spectra in the presence of sea slicks is observed in comparison with those of clean sea surfaces. Moreover, the Doppler spectra of contaminated sea surfaces with oils of types B and C are narrower than those of clean sea surfaces. This is attributed to the fact that the Doppler spectrum width depends primarily on the variance of orbital velocities. The oil slick damping decreases the magnitude of the sea surface roughness spectrum and thus decreases the variance of sea surface orbital velocities. This narrowing effect was confirmed in wind-wave tank measurements[29] performed at a fixed incidence angle of 35 deg using an X-band radar. It should be noted that our simulations are performed at the S-band (3 GHz), while the measurements are performed at the X-band. Thus, we cannot fairly compare our simulation results with measurements.[29] Qualitatively speaking, our simulation results are consistent with measurements.[29]

In comparison with Doppler spectrum width, the variation tendency of Doppler spectral peaks is more complicated. As illustrated in Figs. 7 and 8, the Doppler spectral peaks in the presence of sea slicks can be shifted to higher or lower frequencies relative to the corresponding clean sea surfaces, dependent on incidence angle and oil property. More specifically, the Doppler spectral peaks are shifted to higher frequencies for small to moderate incidence angles ($\theta_i < 30$ deg), which is qualitatively consistent with measurements performed at about an angle of 20 deg incidence using an X-band radar.[41] The measurements[41] conducted in the Black Sea show that the Doppler spectra obtained from slick-covered regions showed strong shifts of the mean Doppler return toward higher frequencies compared with that obtained from slick-free areas.

As incidence angle increases, the Doppler spectral peaks in slicks are gradually shifted to lower frequencies compared with those of clean sea surfaces. In particular, for an incidence angle

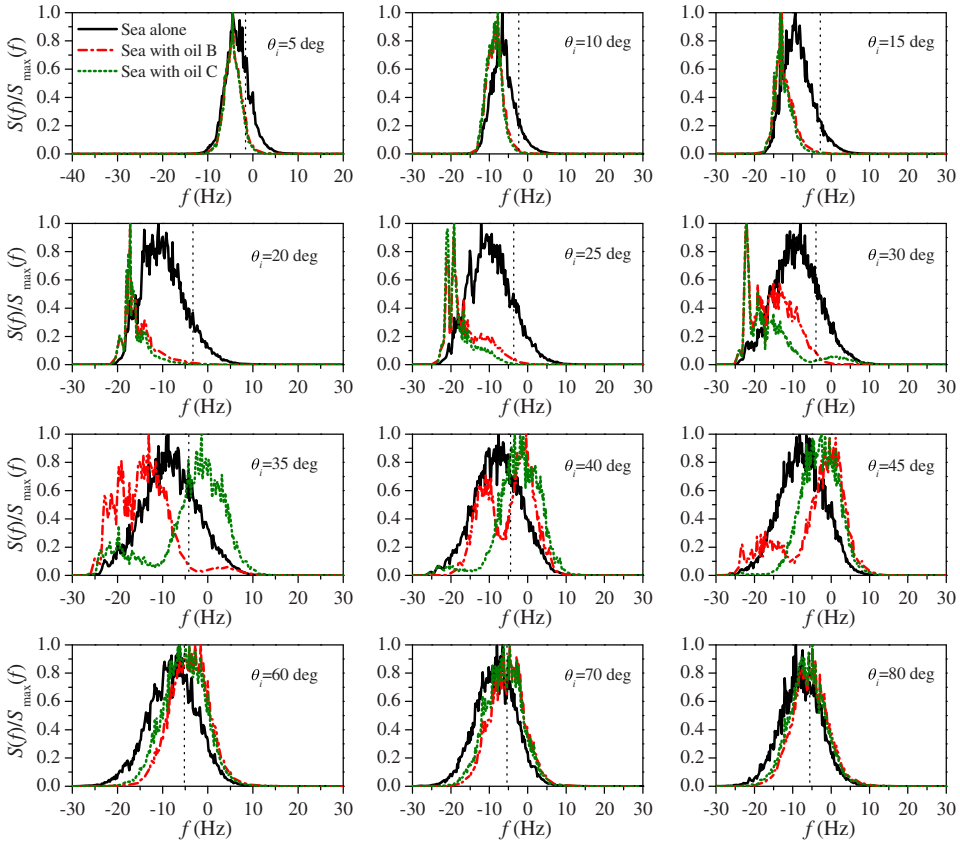

Fig. 8 Same as Fig. 7, but with wind speed $U_{10} = 5$ m/s.

of 35 deg, the Doppler spectral peaks in oil B are shifted to higher frequencies relative to that of clean sea surfaces, whereas the Doppler spectral peaks in oil C are shifted to lower frequencies compared with that of clean sea surfaces. This implies that the variation tendency of the Doppler spectral peak is sensitive to oil properties, which is potentially valuable for the discrimination of oil slicks with different elasticity floating on sea surfaces. In addition, we can observe that the Doppler spectra in oil C are somewhat narrower than those in oil B. This is attributed to the fact that oil C has a stronger damping effect than oil B.

It should be noted that except for wind speed, the same simulation parameters are used in Figs. 7 and 8. Comparing Figs. 7 and 8, one can observe that the Doppler spectra with wind speed $U_{10} = 5$ m/s is somewhat broader than those with wind speed $U_{10} = 3$ m/s. This is attributed to the fact that the orbital velocity of ocean waves with wind speed $U_{10} = 5$ m/s is larger than that with wind speed $U_{10} = 3$ m/s, and that Doppler spectrum width depends primarily on the variance of orbital velocities.

To quantitatively measure the difference between clean and contaminated nonlinear sea surfaces with wind speed $U_{10} = 5$ m/s, the Doppler centroid and spectral bandwidth for VV-polarization versus incidence angle are presented in Figs. 9(a) and 9(b), respectively. The Doppler spectrum in oil of type A with wind speed $U_{10} = 5$ m/s is not presented due to space limitations, but its Doppler shift and spectral bandwidth are shown in Figs. 9(a) and 9(b), respectively. Comparing the Doppler shift of clean and contaminated nonlinear sea surfaces, we can observe that the Doppler shift of radar sea-echo in the presence of sea slicks can decrease or increase as illustrated in Fig. 9(a), which depends on incidence angles and sea slick characteristics represented by the elasticity modulus of oil films. More specifically, the Doppler shift in oil of type A is always larger than that of clean sea surfaces. However, it is indicated that for oils of types B and C, the Doppler shift in slicks is increased for small incidence angles and is decreased for large incidence angles compared with that of clean sea surfaces. It should be noted that oils of types B and C have a stronger damping effect on the small-scale waves of sea surfaces in

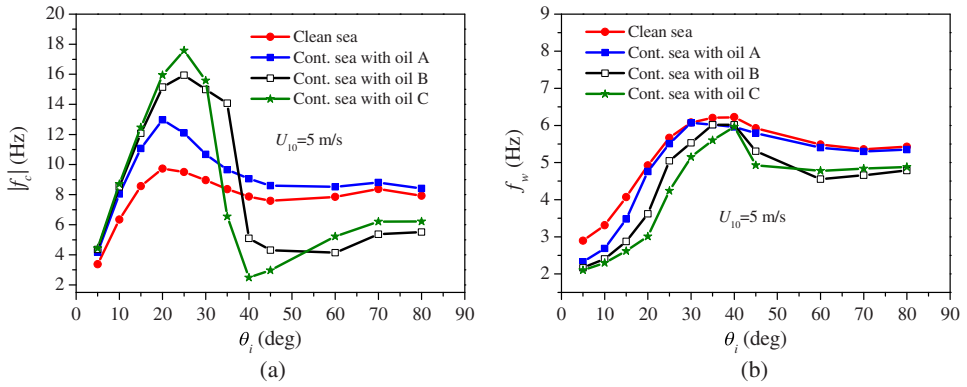

Fig. 9 Comparison of Doppler shifts and bandwidths of clean and contaminated nonlinear sea surfaces with wind speed $U_{10} = 5$ m/s: (a) Doppler shifts and (b) Doppler bandwidths.

comparison with oil of type A, as mentioned in Sec. 2.1. Measurements[27,28] performed at a fixed incidence angle using X- and Ka-band radar showed that Doppler shifts in slicks can increase or decrease, depending on radar wavelength, surface film characteristics, and so forth. However, we cannot fairly compare our simulations with measurements,[27,28] since the simulations in the present study are limited to the S-band (3 GHz) due to computational burden. Nonetheless, the simulation results are qualitatively consistent with the measurements.[27,28] From Fig. 9(b), we can observe that the Doppler spectral bandwidth of contaminated sea surfaces is smaller than that of clean sea surfaces. This is attributed to the fact that the orbital velocity of ocean waves is reduced due to the presence of sea slicks and that the Doppler spectrum width depends primarily on the variance of orbital velocities. Moreover, the Doppler spectral bandwidths in the presence of sea slicks of types B and C are smaller than those in oil of type A. This is due to the fact that oils of type B and C have a stronger damping effect compared with oil of type A. As mentioned previously, the narrowing of the Doppler spectrum in slicks was confirmed in wind-wave tank measurements.[29] Comparing the difference of Doppler spectral bandwidth and Doppler shift between clean and contaminated sea surfaces, we can conclude that Doppler shift is more sensitive to oil properties, which is potentially valuable for discriminating oil films with different elasticity.

4 Conclusion

In this paper, the influence of sea slicks on the bistatic scattering coefficient and Doppler spectrum of radar sea-echo from rough sea surfaces is investigated by comparison with clean sea surfaces. The simulation results show that at normal incidence, the angular distribution of scattering intensity in slicks is more concentrated and higher than that of clean sea surface, and that at moderate incidence angles, the backscattering intensity is reduced, which is qualitatively consistent with measurements. For the Doppler spectrum of radar sea-echo, a narrowing of the Doppler spectrum in the presence of oil slicks is observed, which is qualitatively consistent with wave-tank measurements. In addition, the numerical results indicate that the Doppler shift in slicks can decrease or increase, dependent on incidence angles and oil characteristics, which is qualitatively consistent with open sea measurements. These qualitative results relating to Doppler shift and bandwidth are potentially valuable for remote sensing of sea slicks floating on ocean surfaces, although the present study is limited to 1-D sea surfaces due to the severe computational burden. Moreover, it is possible to discriminate oil films with different elasticities by using the Doppler shift of the radar sea-echo, which is more sensitive to oil film elasticity in comparison with Doppler spectral bandwidth. It needs to be pointed out that the future investigation on this topic will include the Doppler spectrum of radar sea-echo from two-dimensional sea surfaces covered by sea slicks. It should also be pointed out that the discrimination between oil films and look-alikes deserves further investigation, which goes beyond the scope of this paper.

Acknowledgments

This work was supported by the National Science Foundation for Distinguished Young Scholars of China (Grant No. 61225002), and partially by the National Natural Science Funds (Grant Nos. 61301070 and 41406201).

References

1. C. Brekke and A. H. S. Solberg, "Oil spill detection by satellite remote sensing," *Remote Sens. Environ.* **95**(1), 1–13 (2005).
2. F. Nunziata, A. Gambardella, and M. Migliaccio, "On the Mueller scattering matrix for SAR sea oil slick observation," *IEEE Geosci. Remote Sens. Lett.* **5**(4), 691–695 (2008).
3. A. B. Salberg, O. Rudjord, and A. H. S. Solberg, "Oil spill detection in hybrid-polarimetric SAR images," *IEEE Trans. Geosci. Remote Sens.* **52**(10), 6521–6533 (2014).
4. A. H. S. Solberg, "Remote sensing of ocean oil-spill pollution," *Proc. IEEE* **100**(10), 2931–2945 (2012).
5. A. H. S. Solberg, C. Brekke, and P. O. Husy, "Oil spill detection in Radarsat and Envisat SAR images," *IEEE Trans. Geosci. Remote Sens.* **45**(3), 746–755 (2007).
6. G. Franceschetti et al., "SAR raw signal simulation of oil slicks in ocean environments," *IEEE Trans. Geosci. Remote Sens.* **40**(9), 1935–1949 (2002).
7. H. Ghanmi, A. Khenchaf, and F. Comblet, "Numerical modeling of electromagnetic scattering from sea surface covered by oil," *J. Electromagn. Anal. Appl.* **6**, 15–24 (2014).
8. H. Ghanmi, A. Khenchaf, and F. Comblet, "Bistatic electromagnetic scattering and detection of pollutant on a sea surface," *J. Appl. Remote Sens.* **9**(1), 096007 (2015).
9. N. Pinel, N. Déchamps, and C. Bourlier, "Modeling of the bistatic electromagnetic scattering from sea surfaces covered in oil for microwave applications," *IEEE Trans. Geosci. Remote Sens.* **46**(2), 385–392 (2008).
10. M. A. Demir, J. T. Johnson, and T. J. Zajdel, "A study of the fourth-order small perturbation method for scattering from two-layer rough surfaces," *IEEE Trans. Geosci. Remote Sens.* **50**(9), 3374–3382 (2012).
11. X. Y. Duan and M. Moghaddam, "Bistatic vector 3-D scattering from layered rough surfaces using stabilized extended boundary condition method," *IEEE Trans. Geosci. Remote Sens.* **51**(5), 2722–2733 (2013).
12. A. Tabatabaeenejad, X. Y. Duan, and M. Moghaddam, "Coherent scattering of electromagnetic waves from two-layer rough surfaces within the Kirchhoff regime," *IEEE Trans. Geosci. Remote Sens.* **51**(7), 3943–3953 (2013).
13. C. Wu et al., "An accurate and fast forward model of three-dimensional electromagnetic wave scattering in a layered structure with multilayer rough interfaces," *Radio Sci.* **50**(3), 211–228 (2015).
14. H. J. Luo et al., "Numerical studies of sea surface scattering with the GMRES-RP method," *IEEE Trans. Geosci. Remote Sens.* **52**(4), 2064–2073 (2014).
15. D. Miret, G. Soriano, and M. Saillard, "Rigorous simulations of microwave scattering from finite conductivity two-dimensional sea surfaces at low grazing angles," *IEEE Trans. Geosci. Remote Sens.* **52**(6), 3150–3158 (2014).
16. N. Sajjad, A. Khenchaf, and S. A. Mushtaq, "Grazing angle scattering of electromagnetic waves based on an improved two-scale model," *J. Appl. Remote Sens.* **7**(1), 073571 (2013).
17. A. G. Voronovich and V. U. Zavorotny, "Full-polarization modeling of monostatic and bistatic radar scattering from a rough sea surface," *IEEE Trans. Antennas Propag.* **62**(3), 1362–1371 (2014).
18. X. F. Li and X. J. Xu, "Scattering and Doppler spectral analysis for two-dimensional linear and nonlinear sea surfaces," *IEEE Trans. Geosci. Remote Sens.* **49**(2), 603–611 (2011).
19. D. Miret et al., "Sea surface microwave scattering at extreme grazing angle: numerical investigation of the Doppler shift," *IEEE Trans. Geosci. Remote Sens.* **52**(11), 7120–7129 (2014).
20. C. L. Rino et al., "Numerical simulation of backscatter from linear and nonlinear ocean surface realizations," *Radio Sci.* **26**(1), 51–71 (1991).

21. J. V. Toporkov and G. S. Brown, "Numerical simulations of scattering from time-varying, randomly rough surfaces," *IEEE Trans. Geosci. Remote Sens.* **38**(4), 1616–1625 (2000).
22. F. Nouguier, C. A. Guérin, and B. Chapron, ""Choppy wave" model for nonlinear gravity waves," *J. Geophys. Res.* **114**(C9), C09012 (2009).
23. W. Alpers and H. Hühnerfuss, "Radar signatures of oil films floating on the sea surface and the Marangoni effect," *J. Geophys. Res.* **93**(C4), 3642–3648 (1988).
24. M. Gade et al., "On the reduction of the radar backscatter by oceanic surface films: scatterometer measurements and their theoretical interpretation," *Remote Sens. Environ.* **66**(1), 52–70 (1998).
25. H. Hühnerfuss et al., "The modification of X and L band radar signals by monomolecular sea slicks," *J. Geophys. Res.* **88**(C14), 9817–9822 (1983).
26. J. W. Johnson and W. F. Croswell, "Characteristics of 13.9 GHz radar scattering from oil films on the sea surface," *Radio Sci.* **17**(3), 611–617 (1982).
27. S. A. Ermakov et al., "Anormal Doppler shifts of radar signals backscattered from marine slicks," in *Proc. IEEE Int. Geoscience and Remote Sensing Symp.*, Vol. 5, pp. 2986–2988 (2002).
28. S. A. Ermakov et al., "Field observations of radar backscatter modulation and radar Doppler shifts in slicks," in *Proc. of IEEE Geoscience and Remote Sensing Symp.*, Vol. 4, pp. 1513–1515 (2000).
29. M. Gade et al., "Wind-wave tank measurements of bound and freely propagating short gravity-capillary waves," *J. Geophys. Res.* **103**(C10), 21697–21709 (1998).
30. S. A. Ermakov, S. G. Salashin, and A. R. Panchenko, "Film slicks on the sea surface and some mechanisms of their formation," *Dyn. Atmos. Oceans* **16**(3–4), 279–304 (1992).
31. A. Jenkins and S. Jacobs, "Wave damping by a thin layer of viscous fluid," *Phys. Fluids* **9**(5), 1256–1264 (1997).
32. P. P. Lombardini et al., "Modulation of the spectra of short gravity waves by sea surface films: slick detection and characterization with a microwave probe," *J. Atmos. Ocean. Technol.* **6**(6), 882–890 (1989).
33. T. Elfouhaily et al., "A unified directional spectrum for long and short wind-driven waves," *J. Geophys. Res.* **102**(C7), 15781–15796 (1997).
34. L. X. Guo, A. Q. Wang, and C. Chai, "Parallel fast multiple method for electromagnetic scattering from one-dimensional large-scale two-layered rough surfaces for large angles of incidence," *IET Microw. Antennas Propag.* **5**(15), 1813–1821 (2011).
35. L. Tsang et al., *Scattering of Electromagnetic Waves: Numerical Simulations*, Vol. **2**, Wiley-Interscience, New York (2001).
36. P. Liu and Y. Q. Jin, "Numerical simulation of the Doppler spectrum of a flying target above dynamic oceanic surface by using the FEM-DDM method," *IEEE Trans. Antennas Propag.* **53**(2), 825–832 (2005).
37. A. Stogryn, "Equations for calculating the dielectric constant of saline water," *IEEE Trans. Microwave Theory Tech.* **19**(8), 733–736 (1971).
38. K. Folgerø, "Bilinear calibration of coaxial transmission/reflection cells for permittivity measurement of low-loss liquids," *Meas. Sci. Technol.* **7**(9), 1260–1269 (1996).
39. P. H. Y. Lee et al., "Wind-speed dependence of small-grazing-angle microwave backscatter from sea surfaces," *IEEE Trans. Antennas Propag.* **44**(3), 333–340 (1996).
40. W. J. Plant, "A model for microwave Doppler sea return at high incidence angles: Bragg scattering from bound, tilted waves," *J. Geophys. Res.* **102**(C9), 21131–21146 (1997).
41. M. B. Kanevsky et al., "Experimental investigation of Doppler spectra of microwave signals backscattered by sea slicks," in *Proc. of IEEE Int. Geoscience and Remote Sensing Symp.*, Vol. 4, pp. 1530–1532 (1997).

Pengju Yang is currently with the School of Physics and Optoelectronic Engineering, Xidian University, and is working toward his PhD in radio physics. His research interests include computational electromagnetics, electromagnetic scattering from rough surfaces, and remote sensing of oil spills.

Lixin Guo received his MS degree in radio science from Xidian University, Xi'an, China, and his PhD degree in astrometry and celestial mechanics from Chinese Academy of Sciences, Beijing, China, in 1993 and 1999, respectively. He has authored and coauthored 4 books and over 300 journal papers. His research interests include electromagnetic wave propagation and scattering in complex system, computational electromagnetic, and fractal electrodynamics.

Chungang Jia received his BS degree in 2009 from the School of Science, Taiyuan University of Technology, China, and he is currently pursuing his PhD degree at the School of Physics and Optoelectronic Engineering, Xidian University, China. His research interests include GPU high-performance computing in remote sensing and computational electromagnetics.